Article:
Mueller, T, Dohmen, R, Becker, HW et al. (2 more authors) (2013) Fe-Mg interdiffusion rates in clinopyroxene: Experimental data and implications for Fe-Mg exchange geothermometers. Contributions to Mineralogy and Petrology, 166 (6). 1563 - 1576. ISSN 0010-7999

https://doi.org/10.1007/s00410-013-0941-y

Fe-Mg interdiffusion rates in clinopyroxene: experimental data and implications for Fe-Mg exchange geothermometers

by

T. Müller[1], R. Dohmen[1], H.W. Becker[2], Jan H. ter Heege[1,3], and S. Chakraborty[1]

[1] Institut für Geologie, Mineralogie und Geophysik, Ruhr-Universität Bochum, Germany

[2] RUBION, Ruhr-Universität Bochum, Bochum, Germany

[3] TNO – Built Environment and Geosciences, Utrecht, The Netherlands

Keywords: clinopyroxene, diffusion, thin film, geothermometry, geospeedometry, RBS, PLD

Abstract

Chemical interdiffusion of Fe-Mg along the c-axis [001] in natural diopside crystals (X_{Di} = 0.93) was experimentally studied at ambient pressure, at temperatures ranging from 800 - 1200 °C and oxygen fugacities of 10^{-11} to 10^{-17} bar. Diffusion couples were prepared by ablating an olivine (X_{Fo}=0.3) target to deposit a thin film (20 – 100 nm) onto a polished surface of a natural, oriented diopside crystal using the pulsed laser deposition (PLD) technique. After diffusion anneals, compositional depth profiles at the near surface region (~ 400 nm) were measured using Rutherford Backscattering Spectroscopy (RBS). In the experimental temperature and compositional range, no strong dependence of D^{Fe-Mg} on composition of clinopyroxene (Fe/Mg ratio between Di_{93} – Di_{65}) or oxygen fugacity could be detected within the resolution of the study. The lack of fO_2-dependence may be related to the relatively high Al content of the crystals used in this study. Diffusion coefficients, D^{Fe-Mg}, can be described by a single Arrhenius relation with

$$D^{Fe-Mg} = 2.77 \pm 4.27 \times 10^{-7} \exp(-320.7 \pm 16.0 \text{ kJ mol}^{-1} / RT) \text{ m}^2/\text{s}.$$

D^{Fe-Mg} in clinopyroxene appears to be faster than diffusion involving Ca-species (e.g. D^{Ca-Mg}) while it is slower than D^{Fe-Mg} in other common mafic minerals (spinel, olivine, garnet, orthopyroxene). As a consequence, diffusion in clinopyroxene may be the rate limiting process for the freezing of many geothermometers and compositional zoning in clinopyroxene may preserve records of a higher (compared to that preserved in other coexisting mafic minerals) temperature segment of the thermal history of a rock. In the absence of pervasive

recrystallization, clinopyroxene grains will retain compositions from peak temperatures at their cores in most geological and planetary settings where peak temperatures did not exceed ~ 1100 °C (e.g. resetting may be expected in slowly cooled mantle rocks, many plutonic mafic rocks, or ultra-high temperature metamorphic rocks).

Introduction

Clinopyroxene is a common constituent of many igneous, metamorphic and mantle derived rocks and it is frequently found in extra-terrestrial samples (e.g. silicate meteorites from asteroids, the moon and Mars). Chemical compositions of clinopyroxenes are important indicators of magmatic and metamorphic evolution. Partitioning of Fe and Mg between clinopyroxene and many coexisting phases (e.g. orthopyroxene, garnet, olivine, spinel, or melt) is temperature dependent and can be used as geothermometers (e.g., Wood and Banno 1973; Råheim and Green 1974; Wells 1977; Ganguly 1979; Pattison and Newton 1989; Green and Adam 1991; Perkins and Vielzeuf 1992; Loucks 1996; Zack, et al. 1997; Ravna 2002; Putirka, et al. 2003). The fact that clinopyroxenes are frequently chemically zoned additionally opens up the prospect of using these for tracking the thermal evolution in diverse settings. However, their utility in this regard is compromised by the fact that interdiffusion rates of Fe-Mg in clinopyroxenes have not yet been experimentally measured. We have undertaken an experimental study making use of silicate thin films that are tens of nanometers thick, and analytical techniques that can resolve compositional profiles on this scale. In this paper we report diffusion data in the geologically relevant temperature range of 800 – 1200 °C from experiments carried out at atmospheric pressure under controlled oxygen fugacity conditions. We use our diffusion data to evaluate the conditions at which Fe-Mg exchange geothermometers involving

clinopyroxene may be expected to preserve temperatures without resetting; and in cases where resetting does occur, we consider the cooling rate information that might be extracted from the frozen zoning profiles.

Experimental and analytical methods

Experimental setup

Natural crystals of gem quality clinopyroxene (cpx 2, purchased from Excalibur Minerals and reported to be from Rajasthan, India) were used for the diffusion experiments. Representative compositions of the clinopyroxene crystals determined with the electron microprobe at the Ruhr-Universität Bochum are shown in Table 1. The average composition yields $Ca_{0.98}Na_{0.02}Mg_{0.88}Fe^{2+}_{0.02}Fe^{3+}_{0.04}Al^{VI}_{0.04}Si_{1.93}Al^{IV}_{0.07}O_6$. Although the analyses exhibit some heterogeneity in the Al-content, the Fe-Mg ratio seems to be constant and reveals a near end-member Fe-rich diopside composition of Di_{93}. Slices of about 2 mm thickness, approximately perpendicular to the c-axis, were cut out of the original cpx crystals (~ 1cm in diameter). The slices were polished progressively down to finer grit sizes using diamond compounds, followed by a final chemical-mechanical polishing step using colloidal silica. Finally, the polished slices were cut into squares of about 2 mm^2 (surface area of polished side) using a high precision diamond wire saw.

Finding a suitable source material for the diffusion experiments turned out to be problematic. Thin films deposited by pulsed laser deposition are originally amorphous and recrystallize in the early stages of the diffusion anneal, resulting in different microstructures depending on the composition, film thickness and temperature (e.g., Dohmen, et al. 2007; Watson and Dohmen 2010). In our case, thin films of a clinopyroxene composition have poor

wetting properties and on annealing they produce isolated, nanoscale, islands of clinopyroxene (of a different composition) on the surface of the crystal in a "bed of thorns" structure (see Watson and Dohmen 2010; figure 6). Therefore, we chose to use source materials of an olivine composition (Fo_{30}). In our earlier studies (Dohmen, et al. 2007; Dohmen 2008) we have found that olivine thin films produce dense, continuous coverage on a variety of mineral substrates. This was found to be the case for clinopyroxene as well. A dense, polycrystalline (with grain size of about a micrometer) film of Fe-rich olivine therefore acted as the diffusive exchange partner for clinopyroxene (Fig. 1). It is important to note, however, that Dohmen et al. (2007) thoroughly investigated the geometry and chemistry of deposited olivine thin films and found a slight excess in SiO_2, i.e. a systematic deviation in stoichiometry from an ideal olivine. Thus, it is likely that initial recrystallization of the thin film produced some orthopyroxene by the reaction of olivine and excess SiO_2 as observed by Dohmen et al. (2007). There are additional complexities that needed to be addressed in the design of these diffusion experiments. The film thickness had to be optimized such that there was enough material in the films to produce well resolved diffusion profiles, but that the film thickness or profile lengths of Fe were not long enough to be affected by overlap with Ca peaks in a RBS spectrum (see below and fig. 2). After several trials and error, it was found that film thicknesses between 20 and 100 nm fulfill these conditions. Olivine thin films (Fo_{30}) of such thickness were produced by pulsed laser deposition (PLD) in our laboratory following procedures that have been described in detail in Dohmen et al. (2002) and Dohmen et al. (2007). Each deposition run was used to coat 2-6 samples. At least one crystal from each set was used as a reference sample to check the thickness and composition of the deposited layer. Measured thicknesses of thin films of reference samples ranged between 20-60 nm. In an earlier study, Dohmen et al. (2002) demonstrated that there is no detectable variation in composition

and less than 10 % variations in the thickness of the deposited layer within 5 mm^2 for samples placed in different positions in the central part within the vacuum chamber. Prior to the deposition the clinopyroxene crystals were heated up to approximately 600°C in vacuum for 10-15 minutes to degas any volatile adsorbents on the sample surfaces. Deposition times varied typically between 8 and 15 minutes depending on the actual measured intensity of the laser during the coating using a pulsed (10Hz, 20KV) UV laser with a wavelength of 193nm.

Diffusion anneals

Samples were annealed for 10–400 hours at 800–1200°C in gas mixing furnaces at one atmosphere total pressure in a continuous flow of a CO-CO_2 gas mixture under controlled oxygen fugacity. Temperatures were monitored continuously using a type B thermocouple and uncertainties arising from both, accuracy of the thermocouple as well as temperature variations during an experimental run, fall within ±2°C. Counting the diffusion anneal time was started when the run temperature of an experiment was reached. This was typically achieved within less than 10 minutes of insertion of the sample in the furnace. The time to attain anneal temperatures is assumed to be negligibly small compared to the overall run durations and no corrections are made for this. The oxygen fugacity was measured with a fO_2-sensor made of yttria stabilized zirconia and is accurate within ±0.1 log units. Experiments were carried out at different partial pressures of oxygen between $1x10^{-11}$ to $1x10^{-17}$ bar over a range of temperatures. A summary of the experiments and details of the run conditions are provided in table 2. In order to test the reproducibility of our results, we performed a time series of experiments at 1000°C (6 – 40 hours; fig. 3). A "zero-time" experiment (heating up to 1000 °C and removing the crystal instantaneously from the furnace) was carried out to test if any modifications of the film

occurred during heating and cooling. After the diffusion anneals, samples were quenched by removing them from the furnace and cooling in air. The crystals were washed in an ultrasonic bath with distilled water, acetone and ethanol to clean the surface and run products were eventually inspected optically before measuring concentration profiles using RBS.

Rutherford Backscattering Spectroscopy (RBS)

In order to measure the nanoscale diffusion profiles that were induced in our experiments we used the non-destructive method of Rutherford Backscattering Spectroscopy (RBS) that allows both, the composition profile as well as the thickness of the film to be determined (see Feldmann 1986 for a review of the method). RBS analyses for this study were performed at the Dynamitron Tandem Accelerator facility of RUBION at the Ruhr-Universität Bochum. We used a 2 MeV beam of α-particles that was focused onto the sample surface using a final aperture of 0.5 mm in diameter. This setup allows measuring profiles from a surface area as small as 1 mm^2 on the polished sample. Acquisition conditions were chosen as follows: The beam current was in a range between 20 and 50 nA. The back-scattered particles were detected at an angle of 160° at an energy resolution of 16 – 20 keV. The sample was tilted slightly relative to the beam (~5°) for the acquisition to avoid channeling along a crystallographic axis. Concentration-depth profiles of Fe and Ca were extracted using the program RBX (Kótai 1994). Representative spectra and concentration-depth profiles (up to 400 nm) for Fe extracted from them are shown in Fig. 2&4 for a sample before and after the diffusion anneal. A detailed description of the procedure followed for processing of RBS data in our laboratory is available in Dohmen et al. (2002; 2007).

Determining diffusion coefficients

The diffusion profiles in our experiments develop due to diffusion from a finite source of known concentration and thickness into an infinite medium with known initial concentration. There are possibilities that (a) diffusion rates in the film and the medium (Cpx) are different, (b) there is a compositional jump due to element partitioning at the film / crystal interface, and (c) diffusion rates are dependent on the concentration of the diffusing species i.e. Fe and Mg in this case. Additionally, if there is a compositional jump due to element partitioning at the film / crystal interface, the possible role of convolution in smearing out this discontinuity (Ganguly, et al. 1988) needs to be accounted for. Lovering (1936) developed an analytical solution for the simplified case of no compositional dependence of diffusivity and no partitioning between the film and substrate (K_D=1) (see also Watson and Dohmen 2010 (eqns. 5-7) for details):

$$\frac{C_f(x,t)-C_s^0}{C_f^0-C_s^0}=-\frac{1+p}{2}*\mathrm{erf}\left(\frac{x}{2\sqrt{D_f t}}\right)+\left(\frac{1+p}{2}\right)*\sum_{n=1}^{\infty}(-p)^{n-1}\left[\mathrm{erf}\left(\frac{dn+x}{2\sqrt{D_f t}}\right)-p*\mathrm{erf}\left(\frac{dn-x}{2\sqrt{D_f t}}\right)\right]$$

and the equivalent expression for the concentration in the substrate (s):

$$\frac{C_s(x,t)-C_s^0}{C_f^0-C_s^0}=-\frac{1+p}{2}*\mathrm{erf}\left(\frac{x}{2\sqrt{D_s t}}\right)+\left(\frac{1+p^2}{2}\right)*\sum_{n=1}^{\infty}(-p)^{n-1}\mathrm{erf}\left(\frac{d\sqrt{D_s/D_f}\,n+x}{2\sqrt{D_s t}}\right)$$

With: $$p:=\frac{\sqrt{D_f}D_s-\sqrt{D_s}D_f}{\sqrt{D_f}D_s+\sqrt{D_s}D_f}$$

These equations can be used to calculate concentration profiles in the film (f) and substrate (s) for the known initial concentrations at time = 0 (C_f^0 and C_s^0) and run durations (t), with diffusion coefficients (D_f and D_s) as the only variable(s) (using d = 2 * film thickness.). The calculated profiles may then be compared with the measured profiles and the diffusion coefficients varied until the best possible description of the measured profile shape is obtained. Alternately, numerical finite difference schemes may be used to calculate simulated profiles accounting for features such as partitioning at the film / crystal interface, convolution, and different diffusion rates in the film and the crystal. We have used both approaches to study the implications for retrieved diffusion coefficients (Fig. 4a).

On the one hand, it is shown that the entire profile, i.e. the segment within the substrate as well as that within the thin film can be nicely described by the analytical solution given above and the diffusion coefficient in the clinopyroxene can be determined. Such a solution is shown in figure 4a for sample 07-CPX-05. On the other hand, the measured Ca and Fe concentrations within the thin film permit the possibility that there is a compositional jump at the interface, and mixed analyses (i.e. convolved profiles) are extracted from the RBS spectra in the area around the interface. Plotting the data on a ternary diagram to visualize the exchange vectors (Fig. 4b) underscores this possibility. Hence, the extracted profile might also be the result of convolution of a profile showing a compositional jump due to element partitioning at the interface. Given that the thin film is a mixture of olivine + orthopyroxene, it is difficult to calculate an exact partition coefficient. However, the extracted profile gives the concentration in atomic percent iron in the thin film or the substrate respectively. Hence, the apparent partition coefficient between bulk thin film and substrate can be defined as

$$K_P^{Fe} = \frac{\text{at.\%Fe}^{\text{film}}}{\text{at.\%Fe}^{\text{substrate}}}$$

For a given stoichiometry, as in the case of clinopyroxene substrate, this can be translated into atoms per formula unit as shown in figure 4b. The thin film, in contrast, consists of a mixture of olivine and orthopyroxene and thus the relative proportions of ol and opx as well as the different atomic ratios based on mineral formula needs to be taken into account. Therefore, we have explored the effects of somewhat extreme values of the effective partition coefficient ranging between 2 and 4 within the temperature range of the experiments. A hypothetical profile calculated using a finite difference scheme with the same, known initial concentrations, fast diffusion in the thin film, and a partition coefficient of 2 at the interface is shown in figure 4a. The profile is convolved for an effective spatial resolution of 20 nm (= 1σ), and compared to the measured data as well as the analytical solution for the simplified case in figure 4a. It is found that while the overall profile shapes differ in detail, most of the difference lies in how compositions within the thin film are described. In particular, the diffusion coefficient in clinopyroxene is constrained primarily by the length of the profile within the clinopyroxene, and the values retrieved using the two approaches are indistinguishable from one another. This insensitivity to the choice of boundary conditions arises in this case because the film is thin, and the difference between profiles calculated using the two sets of boundary conditions are not pronounced (Fig. 4a). Therefore, we have used the analytical solution to determine diffusion coefficients from all our experimental runs and the results are reported in Table 2.

We have analyzed some of the samples before and after the diffusion anneals in order to determine the exact thickness of the source layer for each sample, and in order to document its compositional evolution more accurately. This approach served one very critical purpose. Mass balance could be verified for the experimental runs, i.e. the amount of Fe lost from the films was matched by the amount of Fe that was found to have entered the clinopyroxene crystals by diffusion. This is an added, quantitative check (in addition to optical observations and observations of selected samples in SEM) that there are no unaccounted sources / sinks of Fe, i.e. no process other than diffusion (e.g. chemical reaction, precipitate formation) affected our samples. This is important for diffusion studies in clinopyroxene where phenomena such as early partial melting (EPM) and formation of precipitates (Jaoul and Raterron 1994) are known to occur.

Results

Fits to the RBS spectra allowed us to extract compositional profiles of Fe and Ca; compositional profiles of Mg were inferred from stoichiometry. It is found that in almost all experiments, the process we observed was a pure Fe-Mg exchange and therefore, the diffusion coefficient that is determined in these experiments is $D^{Fe\text{-}Mg}$, the chemical diffusion coefficient for Fe-Mg exchange (Fig. 4b). In six experiments out of 23, slight concentration gradients of Ca developed as well, indicating a ternary multicomponent exchange process. However, results from these experiments lie on the same trend as data from all other runs and therefore these are not treated differently in this study. Strictly speaking, an effective binary Fe-Mg diffusion coefficient is obtained from these runs. The ability to describe the observed profile shapes using a constant diffusion coefficient (in the analytical or the numerical solution) for clinopyroxene indicates that

the compositional dependence of diffusivity is limited (not resolvable in the form of asymmetry of profile shapes within the resolution of our measurement) over the range of compositions spanned by the concentration profiles. The compositional range of clinopyroxene for which diffusion coefficients are determined may be obtained by two methods: (a) Using the known film thickness to determine which part of the profile lies within the clinopyroxene and (b) using compositional vectors and assumed partition coefficients, such as those illustrated in Fig. 4b. Using either approach, we estimate the compositional range to be between Di_{93} and Di_{65}. Fe-Mg diffusion coefficient in clinopyroxene appears to be insensitive to composition over this range.

The time series of experiments carried out at 1000 °C (Fig. 3 and Table 2) indicate that reproducibility of diffusion coefficients is within 0.4 log units for our experiments. This is taken to be the uncertainty on the determination of diffusion coefficients in this study. The uncertainty could be a little higher even for runs at lower temperatures with substantially shorter profile lengths or where there is considerably overlap of Fe and Ca signals (e.g. run 07-CPX-06).

All data are plotted on an Arrhenius diagram in figure 5. We find that for experiments carried out at any given oxygen fugacity, diffusion rates decrease systematically with temperature. It is not possible to carry out experiments over the entire temperature range of this study using the same oxygen fugacity because neither the stability of clinopyroxene (as a function of fO_2) nor the range of fO_2 accessible by mixing CO and CO_2 (experimental constraints of our system) permit that. Within the uncertainties quoted above, diffusion coefficients determined at different fO_2 at a single temperature (950, 1000, 1100 °C) are similar to each other (Table 2, Fig. 6), Therefore, we consider log $D^{Fe\text{-}Mg}$ to be insensitive to fO_2 between $fO_2 = 1 \times 10^{-11}$ and 1×10^{-17} bar within the resolution of this study. Diffusion coefficients from experiments at all oxygen fugacities were considered together to obtain the temperature dependence of diffusion

coefficients. All data obtained between 800 – 1200 °C could be fitted to a single Arrhenius expression [$D = D_0 \exp(-Q/RT)$, where D_0 is a pre-exponential factor and Q is an activation energy, R is the universal gas constant and T is the absolute temperature] to yield D_0 = 2.77 (±4.27) $x10^{-8}$ m^2/sec and Q = 320.7 (±16.0) kJ/mol. The fit, with an estimated uncertainty envelope, is shown in figure 5b. Within the temperature range of the experiments, the Arrhenius expression reproduces the measured diffusion coefficients within 1 log unit. These parameters are valid for Fe-Mg diffusion along the c-axis of a clinopyroxene crystal. Previous studies have found some anisotropy for Mg and Ca tracer diffusion (Zhang, et al. 2010), but diffusion along c-axis is always fastest. Possible effects of diffusion anisotropy have not been explored in this study.

Comparison with previous studies

In spite of the wide interest in the diffusion rates of Fe-Mg in clinopyroxenes (e.g., Frost and Chacko 1989; Pattison, et al. 2003; Krogh Ravna and Terry 2004), no direct experimental determination of this rate is available for comparison. Comparison of profile lengths in clinopyroxene crystals coexisting with crystals of garnet, olivine or orthopyroxene (Smith and Wilson 1985) or inferences from the width of exsolution lamellae in natural pyroxenes from the Bushveld complex (Rietmeijer and Champness 1982; Rietmeijer 1983) indicate that diffusion in clinopyroxene is expected to be slow compared to other ferromagnesian minerals. Rietmeijer (1983) estimates the value of $D^{Ca-(Fe-Mg)}$ to lie between 6 x 10^{-24} and 2 x 10^{-21} m^2/s at 900 °C, which is consistent with the results of this study (Fig. 5, Table 2). A compilation and discussion of all diffusion data in clinopyroxene is available in Cherniak and Dimanov (2010). Experimental studies of chemical diffusion of major divalent elements in clinopyroxene that

could be compared to the results of the present study include Ca-(Mg+Fe) (1100 - 1250 °C; Brady and McCallister 1983), (Fe+Mn)-Mg (900 - 1240 °C; Dimanov and Sautter 2000; 1000 - 1200 °C; Dimanov and Wiedenbeck 2006) and Ca-Mg (950 - 1150 °C; Zhang, et al. 2010). In addition, there is one study published in abstract form, which gives a single value of Ca-(Mg+Fe) interdiffusion at 1100 °C (Fujino, et al. 1990). All of these data are compared in figure 7.

Our results are practically identical to the data of Dimanov and Wiedenbeck (2006) ((Fe+Mn)-Mg) diffusion) within the experimental range, although the activation energy obtained by them from experiments carried out over a smaller temperature range is slightly lower (297 kJ/mol vs. 320 kJ/mol in this study). However, these authors observed a dependence of the interdiffusion coefficient on fO_2 (Fig. 6), which is in contrast to our results. Dimanov and Wiedenbeck (2006) found the (Fe,Mn)-Mg interdiffusion coefficients to be independent of fO_2 only at partial oxygen pressures above 1×10^{-7} or below 1×10^{-15} bar. In the range in between, their experimental results indicate a decrease of the diffusion coefficients by about two log units with decreasing fO_2. We plotted their data points for (Fe,Mn)-Mg interdiffusion at 1100 °C in figure 6 for comparison with our data. Inspection of figure 6 reveals that extracted diffusion coefficients from our experiments (Fe-Mg interdiffusion at 1100 °C with $\log D^{Fe\text{-}Mg} \approx -18.7$ at $fO_2 = 1 \times 10^{-11}$ bar) are practically indistinguishable from their value ($\log D^{(Fe,Mn)\text{-}Mg} = -18.65$) at $fO_2 = 1 \times 10^{-9}$ bar. Furthermore, the derived diffusion coefficients are in agreement with their data even for oxygen fugacities $\geq 1 \times 10^{-11}$ bar if the analytical uncertainties are taken into account. They explained the observed dependence of diffusivity on fO_2 using a point defect model in which, simply speaking, Fe^{2+} oxidizes with increasing fO_2 to form Fe^{3+} and a vacant metal site to maintain charge balance. Consequently, diffusion rates increase with fO_2, and the fO_2-

dependence is a function of the iron-content of clinopyroxene. We note that the Fe-content of the clinopyroxenes used as starting materials in our study and those of Dimanov and Wiedenbeck (2006) are very similar. On the other hand, there is a marked difference in the Al content of the pyroxenes used in the two studies. Incorporation of tetrahedrally coordinated Al in the clinopyroxene structure needs to be charge balanced, for example, by the presence of Fe3+ on the octahedrally coordinated metal sites. In the event that high Al-concentrations are dominantly charge balanced by Fe^{3+} in the initial clinopyroxene structure, variation of fO_2 and the resulting change in concentration of Fe^{3+} does not have any significant influence on vacancy concentrations and hence, on diffusion rates. Our clinopyroxene contains ~0.1 atoms of Al per formula unit, whereas the starting material used by Dimanov and Wiedenbeck (2006) is almost Al-free. It is therefore likely, that the difference in fO_2 dependence of diffusion rates observed in the two studies may be attributed to the different Al-contents of the pyroxene crystals used in the two studies. The higher Al content of the pyroxenes used by us would have produced charge compensating Fe^{3+} that overwhelmed the concentration of vacancies generated by oxidation of Fe^{2+}. If this explanation is correct, then in the terminology of Dohmen and Chakraborty (2007), diffusion in the study of Dimanov and Wiedenbeck (2006) was in the transition metal extrinsic (TaMED) regime whereas diffusion in our study was by a pure extrinsic diffusion mechanism (PED). An experimental study with pyroxene crystals containing a range of Al-contents for the same (or similar) Fe-contents would help to clarify and quantify this aspect.

Ca-(Mg+Fe) or Ca-Mg exchange in clinopyroxene (Brady and McCallister 1983; Zhang, et al. 2010) appear to be consistently slower than Fe-Mg exchange rates within the temperature ranges of measurement. Arrhenius fits to data from these studies over smaller temperature ranges (1100 – 1250 °C for Brady and McCallister, 1983 and 950 – 1150 °C for Zhang et al., 2010)

yield somewhat different activation energies. As a result, the data of Zhang et al. (2010) would imply that Ca-Mg and Fe-Mg diffusion rates might be similar at temperatures of 900 – 700 °C, which are relevant for metamorphic petrology. At lower temperatures, Ca-Mg diffusion would even be faster than Fe-Mg diffusion according to these results. However, low temperature determinations of Ca-Mg diffusion rates and additional constraints on the activation energy are required for establishing such trends.

It is noteworthy that the data from this study could be described by a single set of Arrhenius parameters over the entire temperature range (800 – 1200 °C) of this study and this range includes the point (1100 – 1150 °C) where breaks in slopes were observed for Ca tracer diffusion in diopside (e.g., Dimanov, et al. 1996). The significance of this break in slope (change in mechanism? Early partial melting?) remains a topic of discussion (e.g. see Cherniak and Dimanov 2010). However, this aspect as well as the comparison with Ca-Mg(+Fe) diffusion rates discussed above indicate that the diffusion behavior of Fe-Mg exchange is distinct from cases where Ca, the larger M2 cation in the pyroxene structure, plays a prominent role. This may bear important implications for the closure of different geothermometers involving cpx, depending on whether Fe-Mg or exchange of a Ca-bearing component is involved.

Fe-Mg diffusion rates in clinopyroxene may be compared with experimentally determined Fe-Mg diffusion rates in related mafic minerals. We compare Fe-Mg diffusion rates in spinel (Liermann and Ganguly 2002), olivine (Dohmen, et al. 2007), garnet (Borinski, et al. 2012) and orthopyroxene (Dohmen et al., in prep.) in figure 8. The data are illustrated for typical X_{Fe}-contents of coexisting mafic minerals and a fO_2 of 1 x 10^{-12} bar where a fO_2-dependence is relevant. It is found that $D^{Fe\text{-}Mg}$ decreases in the order spinel > olivine > garnet ~ orthopyroxene > clinopyroxene. Diffusion in clinopyroxene is therefore rate limiting and may be responsible for

the freezing of many geothermometers (e.g. in eclogites). Similarly, of all the common ferromagnesian minerals, clinopyroxene is expected to preserve the highest temperature record in any given situation.

Implications for geothermometry, geospeedometry and timescales of geological and planetary processes

Compositions of clinopyroxenes are widely used in geothermometers because the partitioning of Fe and Mg between clinopyroxene and common rock forming mafic minerals (e.g. garnet, olivine, spinel, orthopyroxene) and melts often depends strongly on temperature. So it is necessary to identify sets of conditions (peak temperatures, cooling rates, grain size) for which information from the peak of a thermal history would be retained in crystals of clinopyroxene. If the compositions are reset, it is necessary to evaluate by how much. As discussed above, the diffusion rates of Fe-Mg in the exchange partners of cpx may be only slightly (e.g. in orthopyroxene, garnet) or considerably (e.g. olivine, spinel, melt) faster than in cpx. Consequently, a formulation such as Dodson (1973) or its modifications (e.g., Dodson 1986; Ganguly and Tirone 1999) that assumes exchange with an effectively infinite reservoir cannot be used to evaluate the compositional resetting of clinopyroxene. Evaluation of recorded temperatures by element exchange is further complicated by the different grain sizes, modal abundances and transport properties along grain boundaries in natural rocks (e.g., Eiler, et al. 1994). Ganguly et al. (2013) stated in a different context that there is no analytical solution to cover all possibilities that may arise in such a two phase, non-isothermal exchange problem and that it is necessary to use numerical tools. We consider some illustrative examples here using a numerical method to provide some sense of where resetting may be expected. We model

diffusive exchange between two adjacent phases i.e. we assume that there is no / negligible interface resistance. However, Dohmen and Chakraborty (2003) and Müller et al., (2010) have shown that even when the phases exchanging Fe-Mg are not in mutual contact, the development of compositional zoning in a phase such as clinopyroxene will often be determined by the diffusion rates in the phase with the slowest diffusion coefficient i.e. clinopyroxene, for comparable grain sizes and modal abundances of exchanging mineral phases (most common mineralogical situations). Therefore, our results will also be applicable to many situations where diffusive exchange occurs between phases that are not immediately adjacent to each other as in the model calculations.

We solve the diffusion equation

$$\left(\frac{\partial C_{Fe/Mg}}{\partial t}\right)_{\alpha} = \frac{\partial}{\partial X}\left(D^{cpx}_{Fe-Mg}\left(\frac{\partial C_{Fe/Mg}}{\partial X}\right)_{\alpha}\right)$$

in two adjacent phases (where each phase is denoted by α) using a finite difference scheme. The concentration distribution is taken to be initially homogeneous in both phases. Concentrations at the interface between the two phases are set by partitioning using

$$K_D^{grt-cpx} = \frac{\left(Fe/Mg\right)_{grt}}{\left(Fe/Mg\right)_{cpx}} = f(T),$$

where K_D is the equilibrium partition coefficient. For the purpose of this study, we use the temperature and pressure dependent expression for K_D between garnet and clinopyroxene derived by Ganguly et al. (1996). As will be seen below, the choice of garnet as an illustrative

exchange partner allows us to infer the behavior of several other phases. Mass balance is maintained at the interface using

$$D^{grt}_{Fe-Mg}\left(\frac{\partial C_{Fe/Mg}}{\partial X}\right)_{grt} = D^{cpx}_{Fe-Mg}\left(\frac{\partial C_{Fe/Mg}}{\partial X}\right)_{cpx}$$

The temperature and compositionally dependent interdiffusion coefficients for Fe-Mg in garnet have been calculated using the data of Borinski et al. (2012). The Fe-Mg interdiffusion data for cpx are from this study. Concentration profiles are calculated iteratively, where the partition- and diffusion- coefficients are updated at each time step to correspond to the temperature attained at that time according to the prescribed cooling rate. The results are presented as final, frozen concentration profiles (Fig. 9) as well as in the form of temperatures that would be calculated (Fig. 10) using the geothermometer by pairing either the compositions at the core of each crystal (under the assumption that they have not been reset, referred to as core-core temperatures henceforth), or the compositions at the rims of the two crystals (rim-rim thermometry). See Onorato et al. (1981) for more details on the evolution of calculated temperatures at different points of the crystal in such a cooling system.

We consider two examples for peak temperatures corresponding to cases that may arise in mantle (1300 °C) and crustal metamorphic (900 °C) samples, respectively. For our illustrative examples we consider grains that are 0.2, 1, and 4 mm in diameter. Larger grains will retain peak concentrations at the core for longer times whereas smaller grains would be reset sooner. We illustrate the evolution of compositional profiles for cooling rates between 10 °C/my and 1000 °C/my. In our model garnet crystals have an initial X_{Fe} = 0.3 and X_{Mg} = 1-X_{Fe}. Clinopyroxene compositions are chosen to be in equilibrium at the initial temperature of a model calculation.

The boundary conditions in our numerical code imply equilibrium conditions at the interface (i.e. the boundary node) at every time. Therefore, rim compositions for calculating rim-rim temperatures are taken from the first interior node, i.e. about 2-3 μm away from the interface, which is also a reasonable proxy for typical electron microprobe analyses.

Considering the "mantle samples" first, we find that on cooling from 1300 °C the initial, peak compositions are not retained in both garnet and clinopyroxene for even the very fastest cooling rates on the order of 1000 °C/my. For slower cooling rates, garnet homogenizes completely and adjusts compositions to lower temperatures during cooling. As a result, core temperatures of only 1100 °C (for 100 °C/my cooling rate) or lower can be retained; the rim compositions freeze at an even later stage of cooling and indicate temperatures on the order of 900 °C for the cooling rates considered in this study. In contrast, the "crustal samples", commencing cooling from a lower temperature, are able to retain compositions from the peak temperature at the core. For only very slow cooling rates (or for smaller grains, on the order of 200 μm) are the core compositions reset. Rim compositions are reset here as well, and indicate temperatures of 550 – 600 °C for the cooling rates used in our simulations.

We can now use our knowledge of Fe-Mg diffusion rates in other phases (Fig. 8 and discussion above) to evaluate how geothermometers involving those phases may behave. As core compositions in garnets tend to get reset for all but the slowest cooling rates and the lower peak temperature, the core compositions of all phases (e.g. olivine, spinel, melt – all of which have much faster diffusivity) other than orthopyroxene will be reset in most situations (excepting extremely rapid cooling, as in volcanic systems, or where unusually large grain sizes are involved). Opx-Cpx pairs are the most refractory and may preserve compositions from the peak conditions in many cases where the peak temperatures did not exceed 1100 °C.

Summarizing, we can conclude that in the absence of pervasive recrystallization, geothermometers involving clinopyroxene hold the potential to record the peak temperature conditions from most settings, with the exception of a few extremes such as slowly cooled mantle or ultra-high temperature metamorphic samples. Compositional zoning would develop at the rims of clinopyroxenes in these cases, and these offer a window of opportunity for determining the timescale of such high temperature cooling processes. For all but the most rapid cooling rates (e.g. volcanic systems), clinopyroxene rims will show zoning (particularly when modern advances in spatially resolved chemical analysis are considered) and these may be used to infer timescales (e.g. cooling rates) of a variety of processes.

Acknowledgements

This studied was financially supported by grants from the DFG and the Ruhr-Universität Bochum to S. Chakraborty that funded the positions of TM, RD and JTH as well as the running of the experimental petrology and the thin film deposition labs. We gratefully acknowledge the constructive comments of Daniele Cherniak, an anonymous reviewer, and the handling editor Jon Blundy.

Figure and Table captions

Table 1: Representative electron microprobe analyses of natural clinopyroxene crystals used for diffusion experiments. Mineral formulae are calculated based on four cations and six oxygens. Fe^{3+} is calculated as 12-$\sum$ of all positive charges normalized to four cations. Distribution of cations to structural positions assume tetrahedral site to be occupied by Si and Al, M2 site by Ca, Na, and M1 site by $Fe^{2+/3+}$+Mg+Al^{VI}+Mn. (Al^{IV} = 2-Si). Diopside component is computed as X_{Di} = (Mg / Mg+Fe+Mn).

Table 2: Summary of experimental run conditions and determined diffusion coefficients. Source material for the thin film deposition was a synthesized fayalite-rich pellet of olivine stoichiometry (Fo_{30}). See text for more details.

Figure 1: Experimental setup for the Fe-(Ca+Mg) interdiffusion couple. Thin films of olivine (Fo_{30}) were deposited using the pulsed laser deposition technique (PLD) onto a polished surface, perpendicular to the c-axis, of a natural diopside crystal (2x2 mm). Typical thickness of thin films ranged between 20 and 100 nm.

Figure 2: Typical measured RBS spectrum of reference sample (gray) and samples after diffusion anneal (black) of sample 07-CPX-5. Steps correspond to α-particles backscattered by the major species of the sample. The originally high Fe content limited to the depth of the thin film in the reference sample decreases and broadens during the diffusion anneal, indicating a depth penetration by Fe diffusing into the crystal.

Figure 3: Time series of Fe-(Ca+Mg) interdiffusion experiments for diffusion parallel to the c-axis of natural diopside crystals (Di_{93}) performed at 1000 °C and an oxygen fugacity of $1x10^{-16}$ bar. Diffusivities are consistent within 0.4 log units over the investigated time range indicating the absence of other processes such as surface reaction or dissolution-reprecipitation during the experiment. The error of a single analysis is smaller than the symbol size.

Figure 4: A) Extracted profiles for Fe of diffusion experiment 07-CPX-5 for Fe-Mg diffusion in clinoproxene 1000 °C and $fO_2 = 1 \times 10^{-12}$ bar (filled circles). Extracted depth profiles have been fitted with 1) an analytical solution with no partitioning, but different diffusivities in the film and substrate (Lovering 1936) and 2) numerical solution with Fe-Mg partitioning using a $K_p^{Fe} = 2$, fast diffusion in the thin film and convolution due to limited spatial resolution (1σ = 20 nm). Both approaches yield the same extracted interdiffusion coefficient. B) Ca-profiles extracted from diffusion experiments 07-CPX-5 before and after the experiment. C) Ternary diagram showing the chemical composition from the interface towards the center of diopside crystal. Initial compositions of the Ca-

free thin film and the natural cpx crystal are marked with stars. Note the increase in Ca in the region around the interface suggesting the presence of mixed analyses or little diffusion of Ca into the thin film. Clinopyroxene compositions have been normalized to one M-cation, i.e. $MeSiO_3$.

Figure 5: Arrhenius plot summarizing experimental results for Fe-Mg cation diffusion in clinopyroxene. A) Extracted diffusion coefficients as a function of the partial oxygen pressure. Note, that no systematic trend of changes in the diffusivity can be observed within the experimental range of $10^{-17} < fO_2 < 10^{-11}$ bar. B) All data obtained between 800 – 1200 °C can be fitted to a single Arrhenius expression shown with an envelope for the estimated uncertainty. The error of an individual data point is covered by the symbol size.

Figure 6: Plot of extracted Fe-Mg interdiffusion coefficients as a function of the partial oxygen pressures for experiments at 950, 1000, and 1100 °C. Diffusion coefficients are constant within the analytical limits for each temperature and thus, no fO_2-dependence can be observed. This is in contrast to the data of Dimanov and Wiedenbeck (2006) for experiments at 1100 °C, see text for details.

Figure 7: Comparison of interdiffusion data in clinopyroxene. Ca-Mg data from Brady and McAllister are corrected for the pressure effect to 1 atm. Results from Dimanov and Wiedenbeck for (Fe,Mn)-Mg are plotted for an oxygen fugacity of $1x10^{-12}$ bar and are indistinguishable from our result at temperatures above 1000 °C and high oxygen fugacities (fig. 6). Ca tracer diffusion data from Dimanov et al. (1994) and Zhang et al. (2010) show systematically slower diffusivities.

Figure 8: Arrhenius relations for Fe-Mg interdiffusion data in ferromagnesian minerals. Diffusion coefficients decrease in the following order: spinel > olivine > orthopyroxene ~ garnet.

Figure 9: Modeling results showing the development of Fe-zonation during Fe-Mg exchange between garnet and clinopyroxene along a linear cooling path (cooling from two different peak T: 1300 °C and 900 °C to mimic mantle and granulite facies conditions). The numerical model assumes equilibrium at the interface and diffusive fluxes across the interface are constrained by mass balance (see text for details).

Figure 10: Modeling results showing the recorded temperatures for core-core (dashed lines) and rim-rim (solid lines) thermometry using the Fe-Mg exchange between garnet and clinopyroxene with different grain sizes (0.2, 1, and 4 mm) and for a linear cooling path. Note that only very high cooling rates in combination with low peak temperatures (900 °C) will preserve the peak compositions at the core of clinopyroxene crystal.

References

Borinski SA, Hoppe U, Chakraborty S, Ganguly J, Bhowmik SK (2012) Multicomponent diffusion in garnets I: general theoretical considerations and experimental data for Fe-Mg systems. Contributions to Mineralogy and Petrology 164(4):571-586 doi:10.1007/s00410-012-0758-0

Brady JB, McCallister RH (1983) Diffusion data for clinopyroxenes from homogenization and self-diffusion experiments. American Mineralogist 68(1-2):95-105

Cherniak DJ, Dimanov A (2010) Diffusion in Pyroxene, Mica and Amphibole. Reviews in Mineralogy and Geochemistry 72(1):641-690 doi:10.2138/rmg.2010.72.14

Dimanov A, Jaoul O, Sautter V (1996) Calcium self-diffusion in natural diopside single crystals. Geochimica Et Cosmochimica Acta 60(21):4095-4106 doi:10.1016/s0016-7037(96)00250-5

Dimanov A, Sautter V (2000) "Average" interdiffusion of (Fe,Mn)-Mg in natural diopside. European Journal of Mineralogy 12(4):749-760

Dimanov A, Wiedenbeck M (2006) (Fe,Mn)-Mg interdiffusion in natural diopside: effect of pO(2). European Journal of Mineralogy 18(6):705-718 doi:10.1127/0935-1221/2006/0018-0705

Dodson MH (1973) Closure temperature in cooling geochronological and petrological systems. Contributions to Mineralogy and Petrology 40(3):259-274

Dodson MH (1986) Closure profiles in cooling systems. In: Materials Science Forum, vol 7. Trans Tech Publications, Aedermannsdorf, Switzerland, pp 145-153

Dohmen R (2008) A new experimental thin film approach to study mobility and partitioning of elements in grain boundaries: Fe-Mg exchange between olivines mediated by transport through an inert grain boundary. American Mineralogist 93(5-6):863-874 doi:10.2138/am.2008.2671

Dohmen R, Becker H-W, Chakraborty S (2007) Fe–Mg diffusion in olivine I: experimental determination between 700 and 1,200 C as a function of composition, crystal orientation and oxygen fugacity. Physics and Chemistry of Minerals 34(6):389-407

Dohmen R, Becker HW, Meissner E, Etzel T, Chakraborty S (2002) Production of silicate thin films using pulsed laser deposition (PLD) and applications to studies in mineral kinetics. European Journal of Mineralogy 14(6):1155-1168 doi:10.1127/0935-1221/2002/0014-1155

Dohmen R, Chakraborty S (2003) Mechanism and kinetics of element and isotopic exchange mediated by a fluid phase. American Mineralogist 88(8-9):1251-1270

Dohmen R, Chakraborty S (2007) Fe-Mg diffusion in olivine II: point defect chemistry, change of diffusion mechanisms and a model for calculation of diffusion coefficients in natural olivine (vol 34, pg 409, 2007). Physics and Chemistry of Minerals 34:597-598 doi:10.1007/s00269-007-0185-3

Eiler JM, Baumgartner LP, Valley JW (1994) Fast grain-boundary - a FORTRAN-77 program for calculating the effects of retrograde interdiffusion of stable isotopes. Computers & Geosciences 20(10):1415-1434 doi:10.1016/0098-3004(94)90102-3

Feldmann LC (1986) Fundamentals of surface and thin film analysis. North-Holland, New York

Frost BR, Chacko T (1989) The granulite uncertainty principle: limitations on thermobarometry in granulites. The Journal of Geology:435-450

Fujino K, Nachara H, Momoi H (1990) Direct determination of cation diffusion coefficients in pyroxenes. Eos 71:943-944

Ganguly J (1979) Garnet and clinopyroxene solid solutions, and geothermometry based on Fe-Mg distribution coefficient. Geochimica Et Cosmochimica Acta 43(7):1021-1029

Ganguly J, Bhattacharya RN, Chakraborty S (1988) Convolution effect in the determination of composition profiles and diffusion coefficients by microprobe step scans. American Mineralogist 73(7-8):901-909

Ganguly J, Cheng WJ, Tirone M (1996) Thermodynamics of aluminosilicate garnet solid solution: New experimental data, an optimized model, and thermometric applications. Contributions to Mineralogy and Petrology 126(1-2):137-151 doi:10.1007/s004100050240

Ganguly J, Tirone M (1999) Diffusion closure temperature and age of a mineral with arbitrary extent of diffusion: theoretical formulation and applications. Earth and Planetary Science Letters 170(1-2):131-140

Ganguly J, Tirone M, Chakraborty S, Domanik K (2013) H-chondrite parent asteroid: A multistage cooling, fragmentation and re-accretion history constrained by thermometric studies, diffusion kinetic modeling and geochronological data. Geochimica Et Cosmochimica Acta 105(0):206-220 doi:http://dx.doi.org/10.1016/j.gca.2012.11.024

Green T, Adam J (1991) Assessment of the garnet–clinopyroxene Fe–Mg exchange thermometer using new experimental data. Journal of Metamorphic Geology 9(3):341-347

Jaoul O, Raterron P (1994) High-temperature deformation of diopside crystal. 3. Influences of pO2 and SiO2 precipitation. Journal of Geophysical Research-Solid Earth 99:9423-9439 doi:10.1029/93jb03363

Kótai E (1994) Computer methods for analysis and simulation of RBS and ERDA spectra. Nuclear Instruments and Methods in Physics Research Section B: Beam Interactions with Materials and Atoms 85(1):588-596

Krogh Ravna E, Terry MP (2004) Geothermobarometry of UHP and HP eclogites and schists–an evaluation of equilibria among garnet–clinopyroxene–kyanite–phengite–coesite/quartz. Journal of Metamorphic Geology 22(6):579-592

Liermann HP, Ganguly J (2002) Diffusion kinetics of Fe2+ and Mg in aluminous spinel: Experimental determination and applications. Geochimica Et Cosmochimica Acta 66(16):2903-2913 doi:10.1016/s0016-7037(02)00875-x

Loucks RR (1996) A precise olivine-augite Mg-Fe-exchange geothermometer. Contributions to Mineralogy and Petrology 125(2-3):140-150

Lovering TS (1936) Heat conduction in dissimilar rocks and the use of thermal models. Bulletin Geological Society of America 47:87-100

Mueller T, Watson EB, Harrison TM (2010) Applications of Diffusion Data to High-Temperature Earth Systems. Reviews in Mineralogy and Geochemistry 72(1):997-1038 doi:10.2138/rmg.2010.72.23

Onorato P, Hopper R, Yinnon H, Uhlmann D, Taylor L, Garrison J, Hunter R (1981) Solute partitioning under continuous cooling conditions as a cooling rate indicator. Journal of Geophysical Research 86(B10):9511-9518

Pattison D, Newton R (1989) Reversed experimental calibration of the garnet-clinopyroxene Fe—Mg exchange thermometer. Contributions to Mineralogy and Petrology 101(1):87-103

Pattison DRM, Chako T, Farquhar J, McFarlane CRM (2003) Temperatures of granulite-facies metamorphism: constraints from experimental phase equilibria and thermobarometry corrected for retrograde exchange. Journal of Petrology 44(5):867-900

Perkins D, Vielzeuf D (1992) Experimental investigation of Fe-Mg distribution between olivine and clinopyroxene: Implications for mixing properties of Fe-Mg in clinopyroxene and garnet-clinopyroxene thermometry. American Mineralogist 77:774-783

Putirka KD, Mikaelian H, Ryerson F, Shaw H (2003) New clinopyroxene-liquid thermobarometers for mafic, evolved, and volatile-bearing lava compositions, with applications to lavas from Tibet and the Snake River Plain, Idaho. American Mineralogist 88(10):1542-1554

Råheim A, Green DH (1974) Experimental determination of the temperature and pressure dependence of the Fe-Mg partition coefficient for coexisting garnet and clinopyroxene. Contributions to Mineralogy and Petrology 48(3):179-203

Ravna K (2002) The garnet–clinopyroxene Fe2+–Mg geothermometer: an updated calibration. Journal of Metamorphic Geology 18(2):211-219.

Rietmeijer FJ (1983) Inter-diffusion coefficients parallel to the c-axis in iron-rich clinopyroxenes calculated from microstructures. Contributions to Mineralogy and Petrology 83(1-2):169-176

Rietmeijer FJM, Champness PE (1982) Exsolution structures in calcic pyroxenes from the Bjerkreim-Skondal lopolith, SW Norway. Mineralogical Magazine 45:11-24 doi:10.1180/minmag.1982.045.337.02

Smith D, Wilson CR (1985) Garnet-olivine equilibration during cooling in the mantle. American Mineralogist 70(1-2):30-39

Watson EB, Dohmen R (2010) Non-traditional and emerging methods for characterizing diffusion in minerals and mineral aggregates. Reviews in Mineralogy and Geochemistry 72(1):61-105

Wells PR (1977) Pyroxene thermometry in simple and complex systems. Contributions to Mineralogy and Petrology 62(2):129-139

Wood BJ, Banno S (1973) Garnet-orthopyroxene and orthopyroxene-clinopyroxene relationships in simple and complex systems. Contributions to Mineralogy and Petrology 42(2):109-124

Zack T, Foley SF, Jenner GA (1997) A consistent partition coefficient set for clinopyroxene, amphibole and garnet from laser ablation microprobe analysis of garnet pyroxenites from Kakanui, New Zealand. Neues Jahrbuch Fur Mineralogie-Abhandlungen 172(1):23-42

Zhang XY, Ganguly J, Ito M (2010) Ca-Mg diffusion in diopside: tracer and chemical inter-diffusion coefficients. Contributions to Mineralogy and Petrology 159(2):175-186 doi:10.1007/s00410-009-0422-5

Figure 1
Click here to download Figure: Fig1.eps

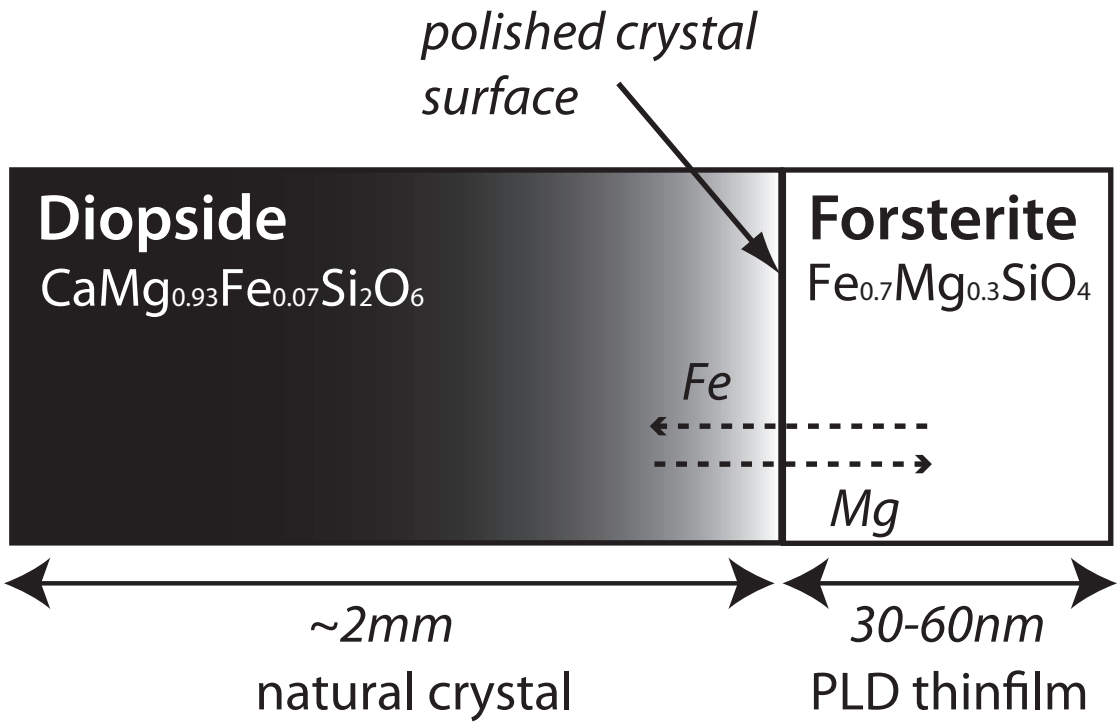

Figure 1
Müller et al. - Fe-Mg diffusion in cpx

Figure 2
Click here to download Figure: Fig2.eps

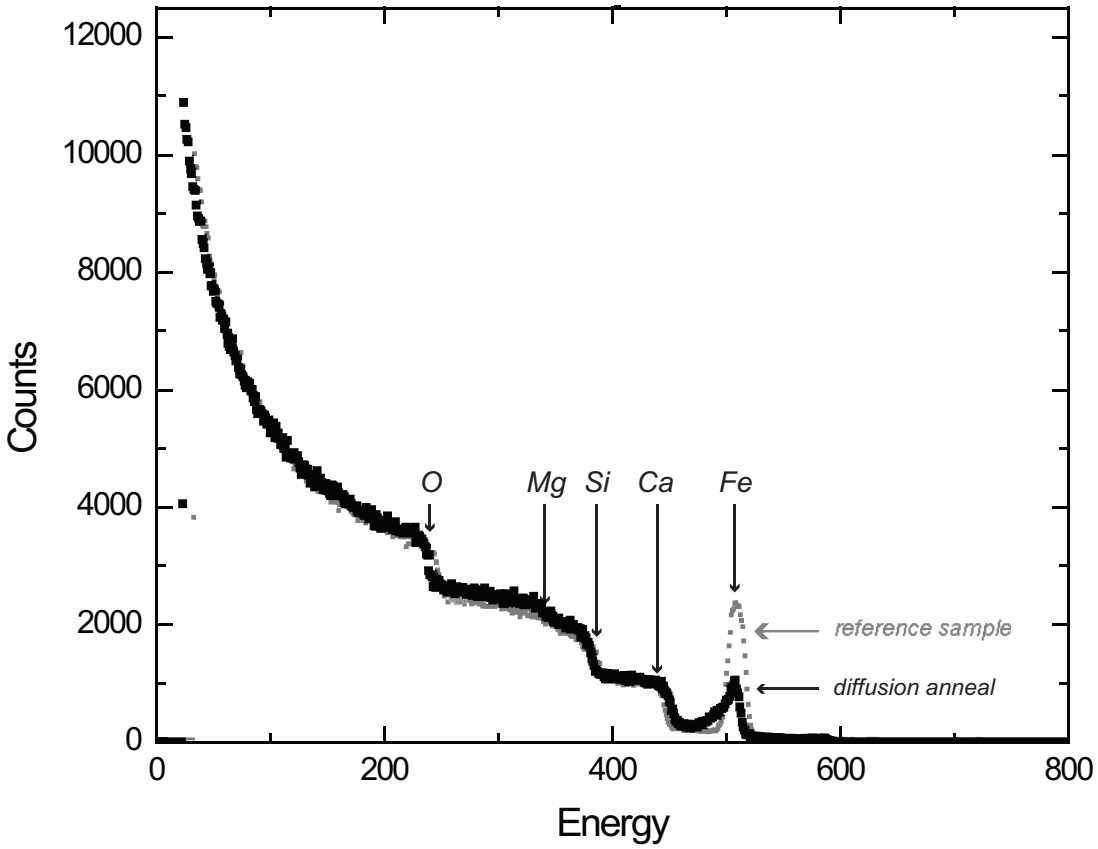

Figure 2
Müller et al. -Fe-Mg diffusion in cpx

Figure 3
Click here to download Figure: Fig3.eps

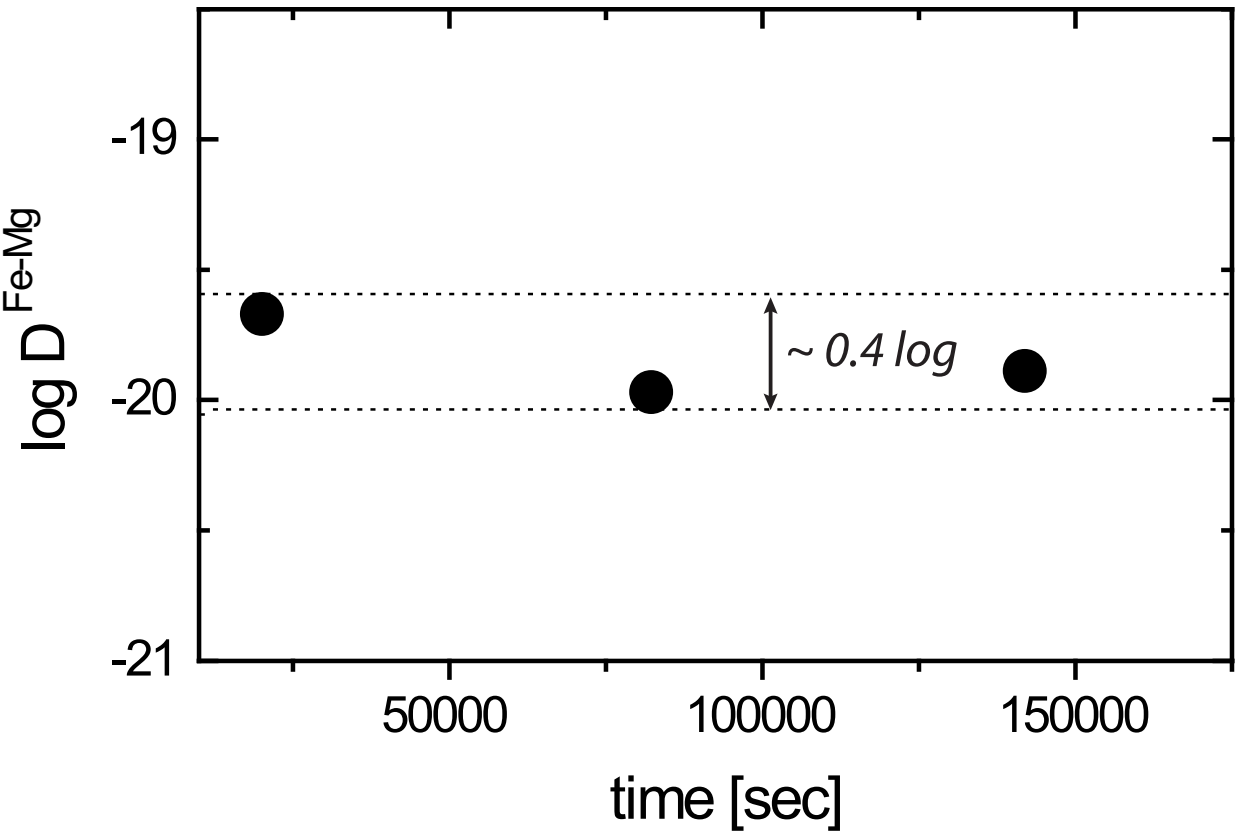

Figure 3
Müller et al. -Fe-Mg diffusion in cpx

Figure 4

Click here to download Figure: Fig4.eps

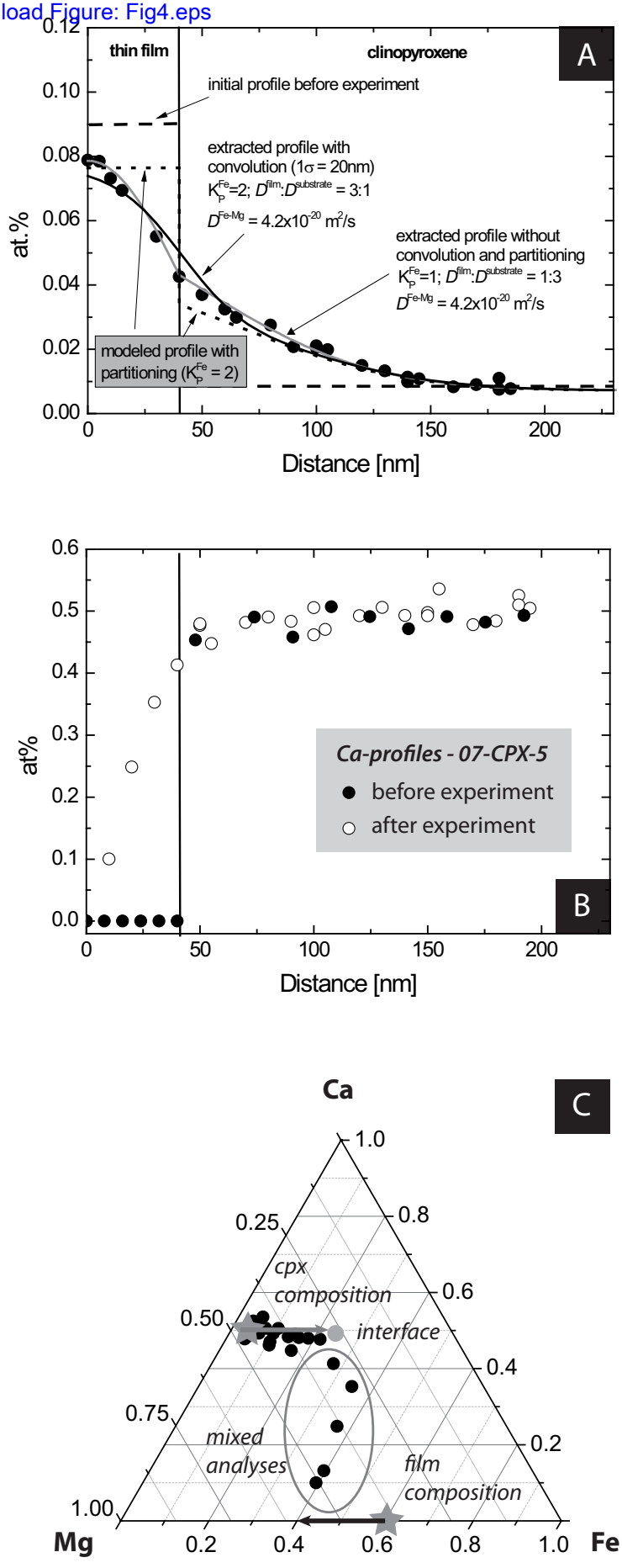

Figure 4

Müller et al. -Fe-Mg diffusion in cpx

Figure 5
Click here to download Figure: Fig5.eps

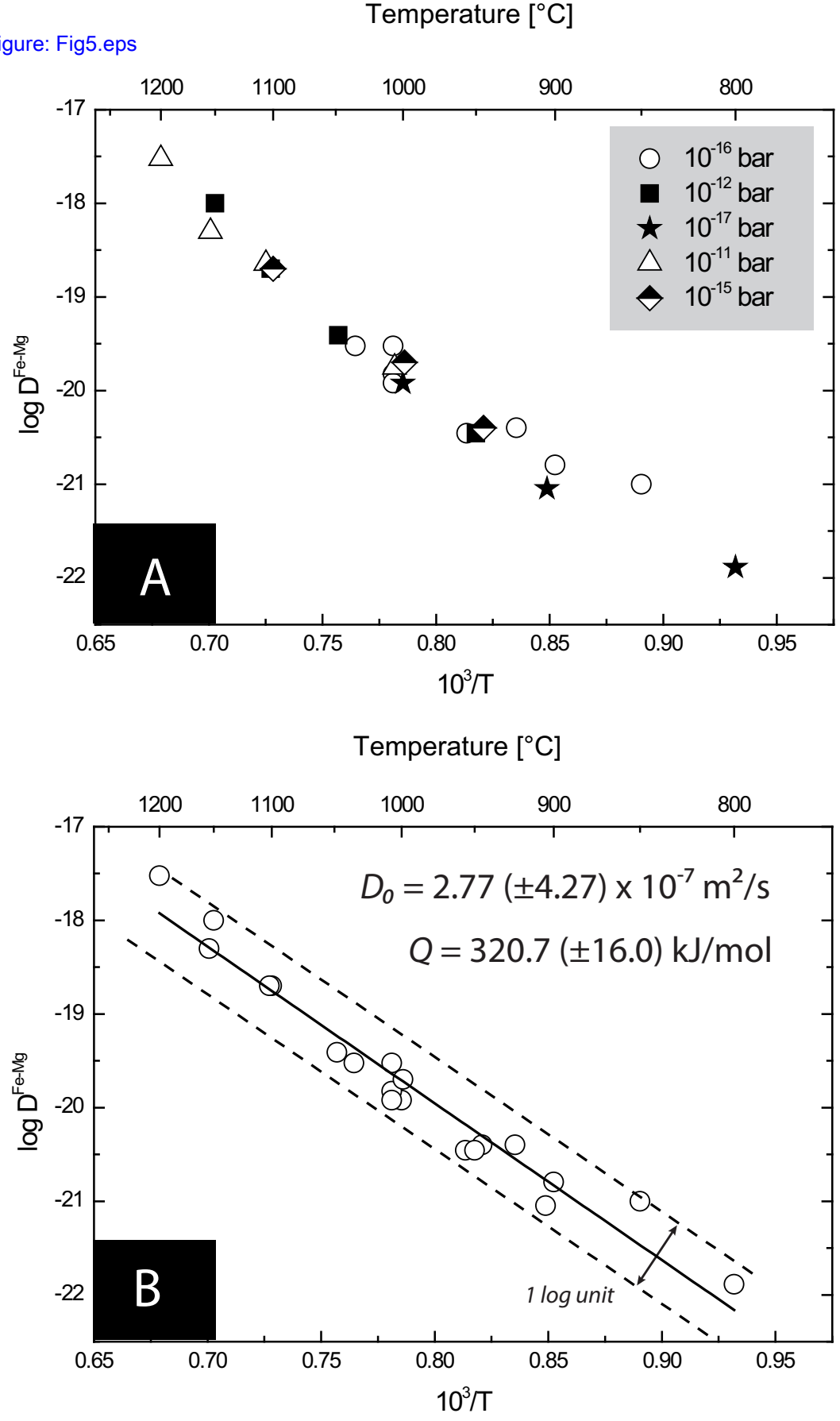

Fig. 5
Mueller et al. - Fe-Mg diffusion in cpx

Figure 6
Click here to download Figure: Fig6.eps

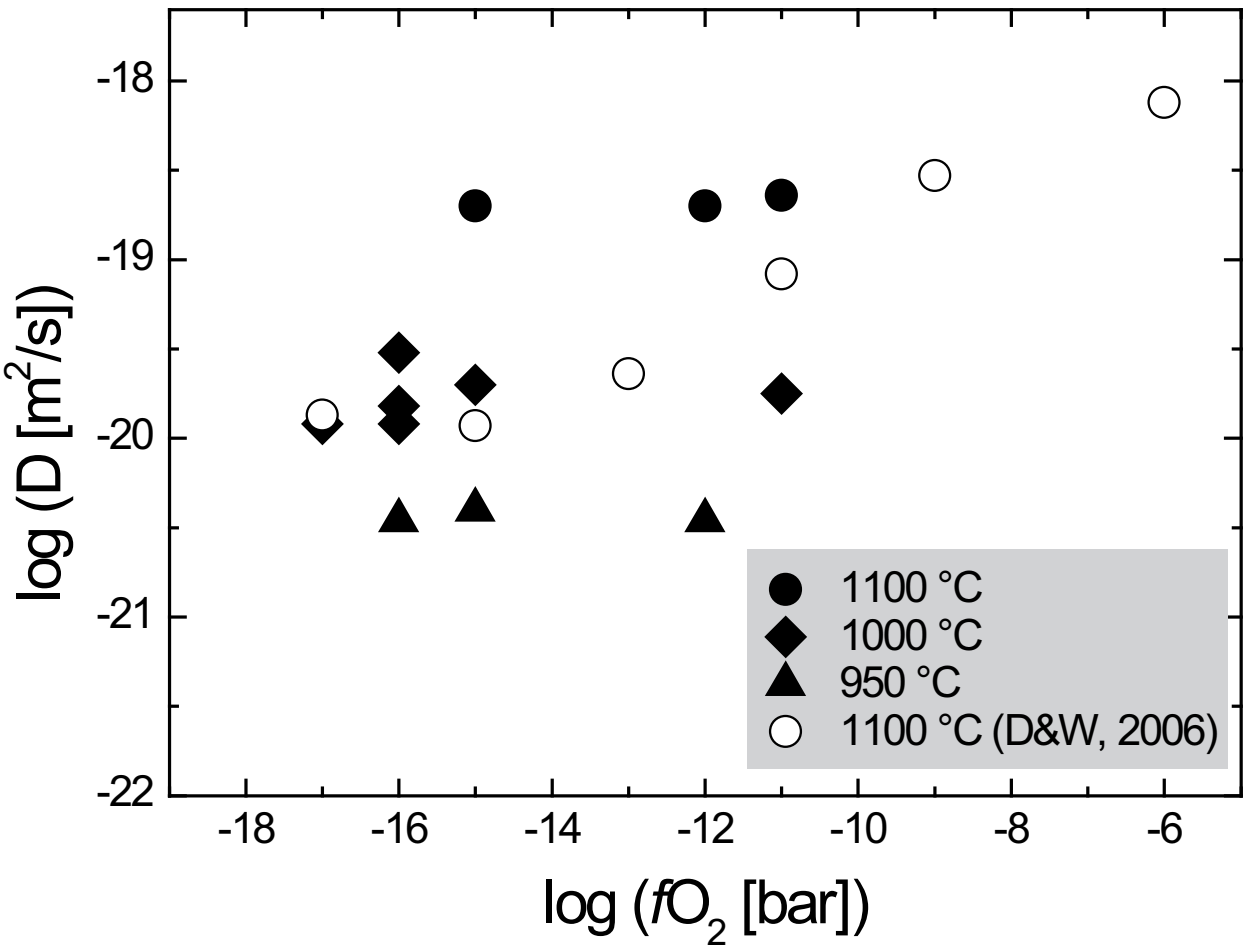

Fig. 6
Mueller et al. - Fe-Mg diffusion in cpx

Figure 7
Click here to download Figure: Fig7.eps

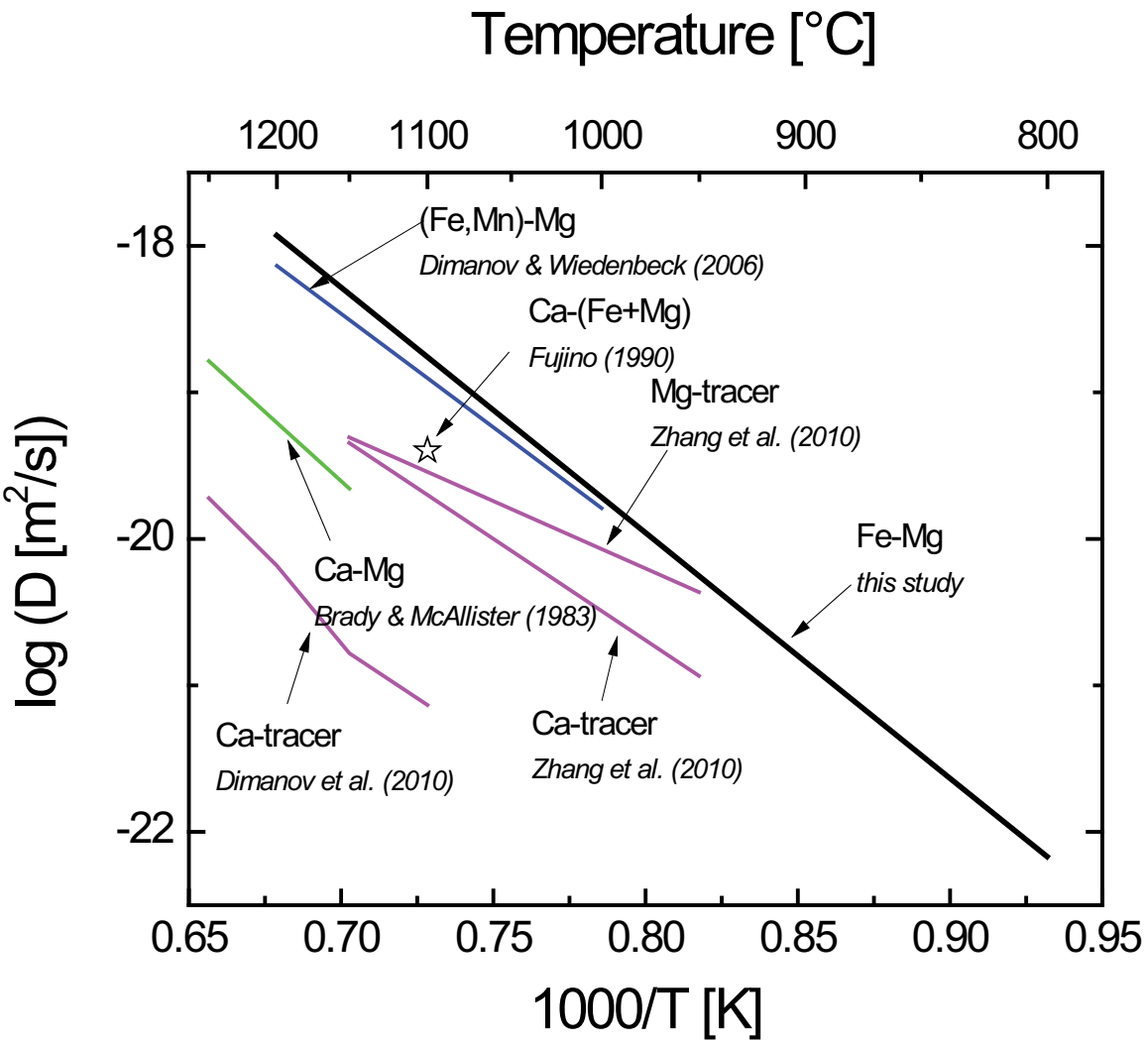

Fig. 7
Mueller et al. - Fe-Mg diffusion in cpx

Figure 8
Click here to download Figure: Fig8.eps

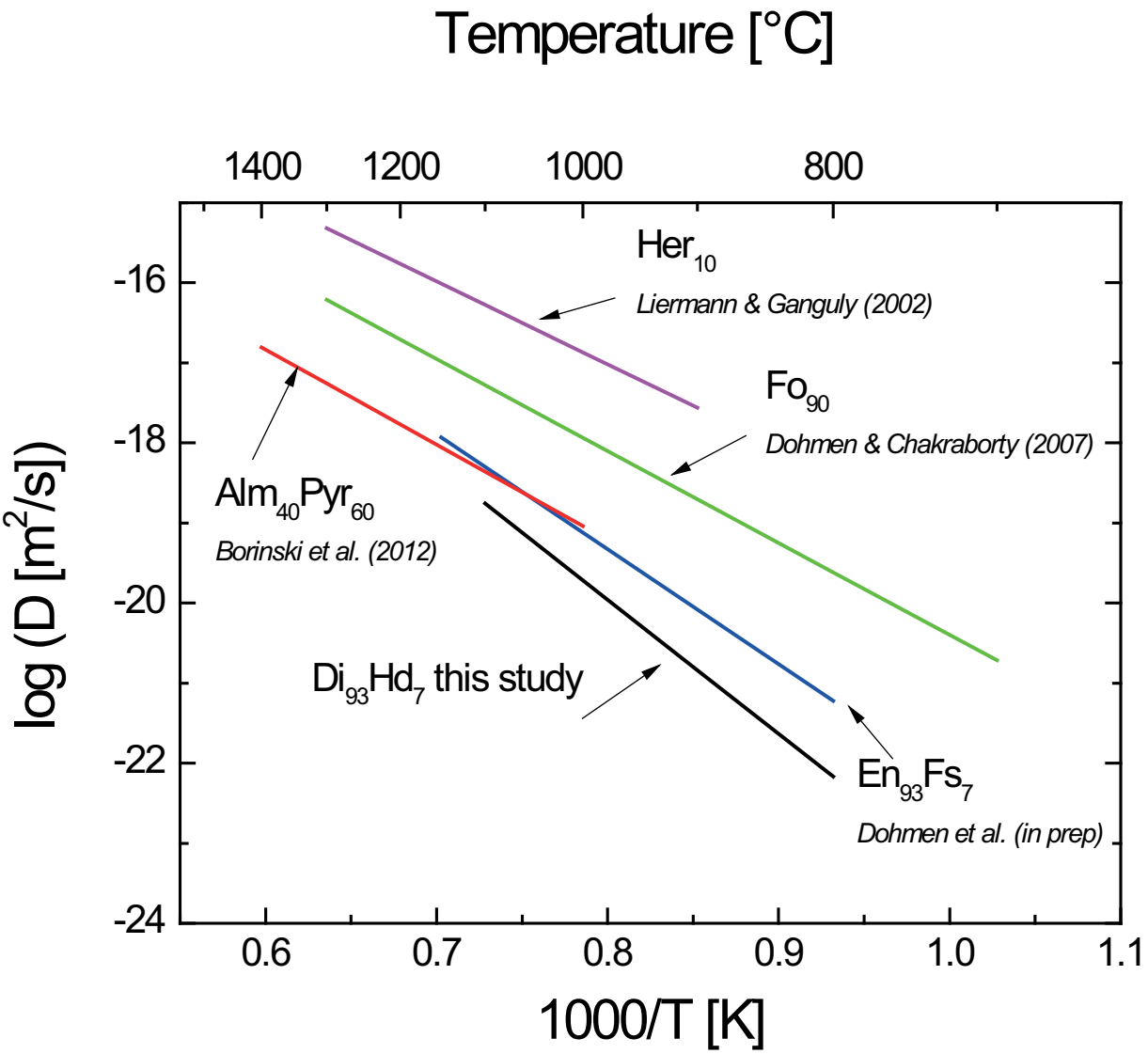

Fig. 8
Mueller et al. - Fe-Mg diffusion in cpx

Figure 9

Click here to download Figure: Fig9.eps

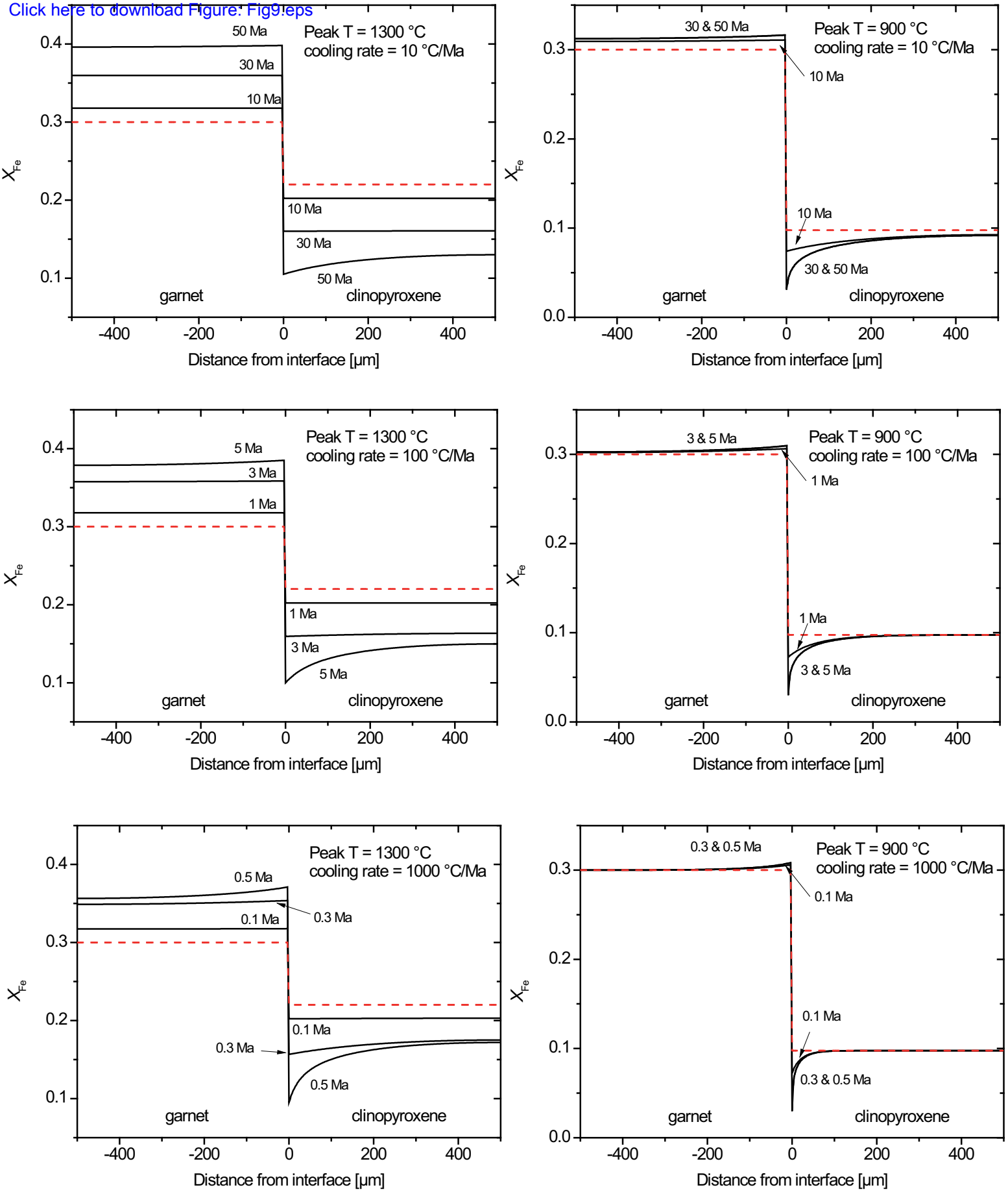

Figure 9

Müller et al. - Fe-Mg diffusion in cpx

Figure 10

Click here to download Figure: Fig10.eps

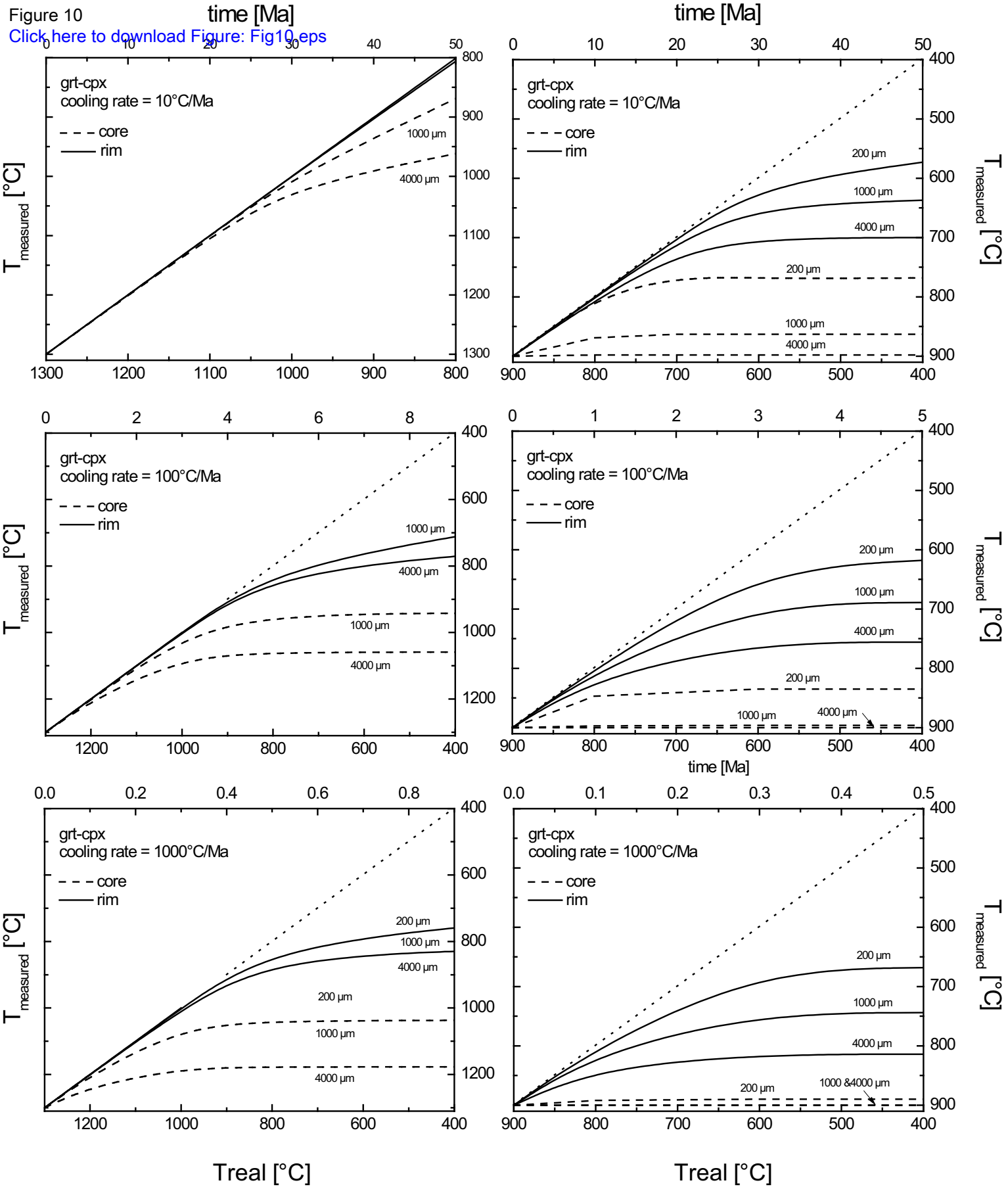

Figure 10

Müller et al. - Fe-Mg diffusion in cpx

table 1

Click here to download table: Table 1 word97.xls

measured wt% Oxide			
SiO2	52.9	52.84	52.65
Al2O3	2.72	2.6	2.65
TiO2	0.11	0.11	0.11
Cr2O3	0.01	0.04	0.03
MgO	15.95	15.99	16.07
FeO	2.21	2.23	2.08
MnO	0.08	0.06	0.08
CaO	25.2	25.08	25.24
Na2O	0.24	0.26	0.2
Total	***99.42***	***99.21***	***99.11***

structural position normalized to 4 cations and 6 oxgens			
Si (T)	1.94	1.93	1.93
AlIV (T)	0.06	0.07	0.07
AlVI (M1)	0.05	0.04	0.04
Ti (M1)	0.00	0.00	0.00
Fe3+ (M1)	0.02	0.05	0.06
Mg (M1)	0.87	0.87	0.88
Fe2+ (M1)	0.04	0.02	0.00
Mn (M2)	0.00	0.00	0.00
Ca (M2)	0.99	0.98	0.99
Na (M2)	0.02	0.02	0.01
X(Di)	**0.93**	**0.93**	**0.93**
X(Hd)	**0.07**	**0.07**	**0.07**

table 2
Click here to download table: Table 2 word97.xls

Experiment	T [°C]	1000/T [K]	t [sec]	log fO2 [bar]	D [m^2/s]	log D [m^2/s]*
07-CPX-01	850	0.890	492000	-16.0	$1.0x10^{-21}$	-21.00
07-CPX-02	900	0.852	264000	-16.0	$1.6x10^{-21}$	-20.80
07-CPX-04	950	0.818	240060	-12.0	$3.5x10^{-21}$	-20.46
07-CPX-06	1150	0.703	4320	-12.0	$1.0x10^{-18}$	-18.00
08-CPX-07	800	0.932	1355820	-17.0	$1.3x10^{-22}$	-21.89
08-CPX-11	905	0.849	423720	-17.0	$9.0x10^{-22}$	-21.05
08-CPX-15	1106	0.725	7200	-11.0	$2.3x10^{-19}$	-18.64
08-CPX-16	1006	0.782	57600	-11.0	$1.8x10^{-20}$	-19.75
08-CPX-17	1154	0.701	3600	-11.0	$5.0x10^{-19}$	-18.30
08-CPX-18	1200	0.679	1800	-11.0	$3.0x10^{-18}$	-17.52
09-CPX-02	1035	0.764	44400	-16.0	$3.0x10^{-20}$	-19.52
09-CPX-03	924	0.835	78600	-16.0	$4.0x10^{-21}$	-20.40
09-CPX-06	1000	0.785	360	-16.0	$1.0x10^{-18}$	*NA*
09-CPX-09	956	0.814	249360	-16.0	$3.5x10^{-21}$	-20.46
09-CPX-11	1048	0.757	31080	-12.0	$3.9x10^{-20}$	-19.41
09-CPX-12	1102	0.727	7440	-12.0	$2.0x10^{-19}$	-18.70
09-CPX-13	945	0.821	225000	-15.0	$4.0x10^{-21}$	-20.40
09-CPX-14	999	0.786	54600	-15.0	$2.0x10^{-20}$	-19.70
09-CPX-15	1100	0.728	9360	-15.0	$2.0x10^{-19}$	-18.70
09-CPX-16	1000	0.785	45240	-17.0	$1.2x10^{-20}$	-19.92
09-CPX-17	1007	0.781	20100	-16.0	$3.0x10^{-20}$	-19.52
09-CPX-18	1007	0.781	82260	-16.0	$1.5x10^{-20}$	-19.82
09-CPX-19	1007	0.781	141600	-16.0	$1.2x10^{-20}$	-19.92

*Uncertainties on log*D* are ±0.2. See figure 3 and text for details.